An Autonomous Tracking and Landing Method for UAV Based on Visual Navigation

Bingkun Wang , Ruitao Ma , Hang Zhu * , Yongbai Sha , Tianye Yang *

Posted Date: 30 October 2023

doi: 10.20944/preprints202310.1777.v1

Keywords: unmanned aerial vehicle; visual navigation; autonomous tracking; dynamic landing

Article

An Autonomous Tracking and Landing Method for UAV Based on Visual Navigation

Bingkun Wang [1], Ruitao Ma [1], Hang Zhu [1,2,*], Yongbai Sha [1] and Tianye Yang [1,2,*]

[1] Key Laboratory of CNC Equipment Reliability, Ministry of Education, School of Mechanical and Aerospace Engineering, Jilin University, Changchun 130022, China; wangbk22@mails.jlu.edu.cn (B.M.); mart23@mails.jlu.edu.cn (R.M.); shayb@jlu.edu.cn (Y.S.)

[2] Chongqing Research Institute, Jilin University, Chongqing 401123, China

* Correspondence: hangzhu@jlu.edu.cn (H.Z.); yangty@jlu.edu.cn (T.Y.)

Abstract: In this paper, we examine potential methods for autonomously tracking and landing multi-rotor unmanned aerial vehicles (UAVs), a complex yet essential problem. Autonomous tracking and landing control technology utilizes visual navigation, relying solely on vision and landmarks to track targets and achieve autonomous landing. This technology improves the UAV's environment perception and autonomous flight capabilities in GPS-free scenarios. In particular, we are researching tracking and landing as a cohesive unit, devising a switching plan for various UAV tracking and landing modes, and creating a flight controller that has an inner and outer loop structure based on relative position estimation. The inner and outer nested markers aid in the independent monitoring and touchdown of UAV. Optimal parameters are determined via optimized experiments on the measurements of the inner and outer markers. An indoor experimental platform for tracking and landing UAV was established. Tracking performance was verified by tracking three trajectories of unmanned ground vehicle (UGV) at varying speeds, and landing accuracy was confirmed through static and dynamic landing experiments. The experimental results show that the proposed scheme has good dynamic tracking and landing performance.

Keywords: unmanned aerial vehicle; visual navigation; autonomous tracking; dynamic landing

1. Introduction

UAVs offer numerous advantages, such as strong maneuverability, low maintenance costs, vertical takeoff ability, and impressive hovering capabilities. As a result, they are widely used in various fields, including search and rescue, exploration, disaster monitoring, inspection, and agriculture [1–4]. However, limitations on payload and flight time significantly restrict the range of UAV missions. Therefore, it is essential to develop fully autonomous multi-rotor UAVs that can collaborate with ground-based robots to perform more complex tasks [5,6]. It is also fraught with considerable challenges. In this case, especially during the takeoff and landing phases, high-precision vehicle position and attitude estimation and motion planning are required [7,8].

In recent years, scholars globally have extensively researched UAV tracking [9,10] and landing techniques [11]. For instance, identifying safe landing locations using visual cues following a severe UAV malfunction [12]. Landing an UAV on an unmanned vessel is a challenging problem [13–15]. The fluctuating water surface causes unpredictable changes in the position and attitude of the unmanned vessel. Landing the UAV on the UGV can give the UGV system the ability to work in three-dimensional space, and carrying the charging module on the UGV can solve the limitations of payload and flight time on the working range of the UAV, but it places high requirements on the accuracy of the drone landing [16–19]. The position and attitude of a UAV is estimated during the landing process, but the position and attitude of today's UAVs are typically measured by inertial measurement units (IMUs) and Global Positioning System(GPS) [20]. However, the positioning

 doi:10.20944/preprints202310.1777.v1

accuracy of GPS is low, and it is not possible to use GPS positioning indoors or in places with a lot of cover. IMUs have the problem of accumulating errors in long-term positioning, making it difficult to perform high-precision tasks such as landing. Therefore, the selection of sensors is particularly important when the UAV performs the landing mission. Laser sensors can provide accurate distance information, accurately calculate the relative position and attitude relationship between the UAV and the landing landmark, and are used in the UAV landing mission [14]. However, laser sensors are expensive, require a large amount of data, and have high platform requirements, making them unsuitable for mounting on small multi-rotor UAVs.

With the advantages of easy maintenance, low price, miniaturization, light weight and low power consumption, vision sensors are widely used in various intelligent robots. With the development of technology, UAV visual localization can provide precise position and angle information, which can meet the accuracy requirements of UAV landing guidance. However, accurate landmark recognition is a challenge, and edge detection algorithms [21,22] and deep learning methods [19] are commonly used. These methods are computationally intensive, poorly portable, and deep learning also requires large amounts of data. Optical flow is also a promising solution for autonomous landing missions [23], but it is less stable as it is highly dependent on the environment.

During UAV landings, as the visual sensor approaches the landing landmark, there is a potential for loss of global and relative position and attitude information, resulting in decreased landing precision or even failure. Therefore, a precise landmark must be designed to steer the UAV towards a successful landing. The use of ArUco marker is a common method for guiding UAV landings [17–19]. When utilizing an ArUco marker for UAV landing guidance, the global information of the marker is forfeited when the UAV landmarks are in close proximity. As a result, nested ArUco markers or ArUco marker matrices are commonly implemented to ensure the precision of the low altitude relative positions and attitudes of the UAV during landing.

The paper's primary contribution is the development of dynamic tracking and landing control strategies for UAV and the optimization of landmark structure and dimensions to obtain the best possible landmark parameters. By relying solely on vision to achieve dynamic tracking and precise landing of UAV, an experimental platform for indoor UAV tracking and landing was established. The UAV tracking performance was validated by tracing three different trajectories of the unmanned ground vehicle (UGV) at varying speeds, while the landing precision of the UAV was confirmed through both static and dynamic landing experiments.

2. Materials and Methods

During the dynamic tracking and landing of the UAV, the state of the UAV is categorized into a tracking mode and a landing mode based on the relative position and attitude of the UAV and the landmark carried by the UGV (shown in Figure 1). The UAV is operated via a control system that features both inner and outer loop structures. The inner loop attitude controller utilizes a fuzzy PID control algorithm to regulate the attitude angle and angular velocity, whereas the outer loop position controller deploys a serial PID control to manage the UAV's position. Initially, the UAV utilizes vision to gather details about the surrounding area. If a landmark is identified, the UAV calculates the relative positions and attitudes of itself and the landmark. If no landmark is detected, the UAV will automatically elevate its altitude to broaden its field of view and locate the landmark. The controller receives the relative position and attitude obtained and translates it into commands to control the UAV. In tracking mode, the UAV sends horizontal channel commands to the UAV's flight controller to steer the UAV horizontally close to landmarks for autonomous UAV tracking, maintaining the UAV's altitude to keep the target in view and adjusting the UAV's speed to keep up with the target. The UAV enters the landing mode when the relative positions and attitudes of the UAV and the landmark meet the landing conditions. In landing mode, the UAV approaches the landmark horizontally, dropping its own altitude and keeping the UGV at the same speed as the tracked target; if the target is lost, it rises to expand the field of view to bring the target back into view; if the target

Preprints (www.preprints.org) | NOT PEER-REVIEWED | Posted: 30 October 2023 doi:10.20944/preprints202310.1777.v1

is not lost, it calculates the straight-line distance to the center of the landmark. When the straight-line distance is less than 0.3m, the UAV's landing command is triggered: the motor stops to land the UAV.

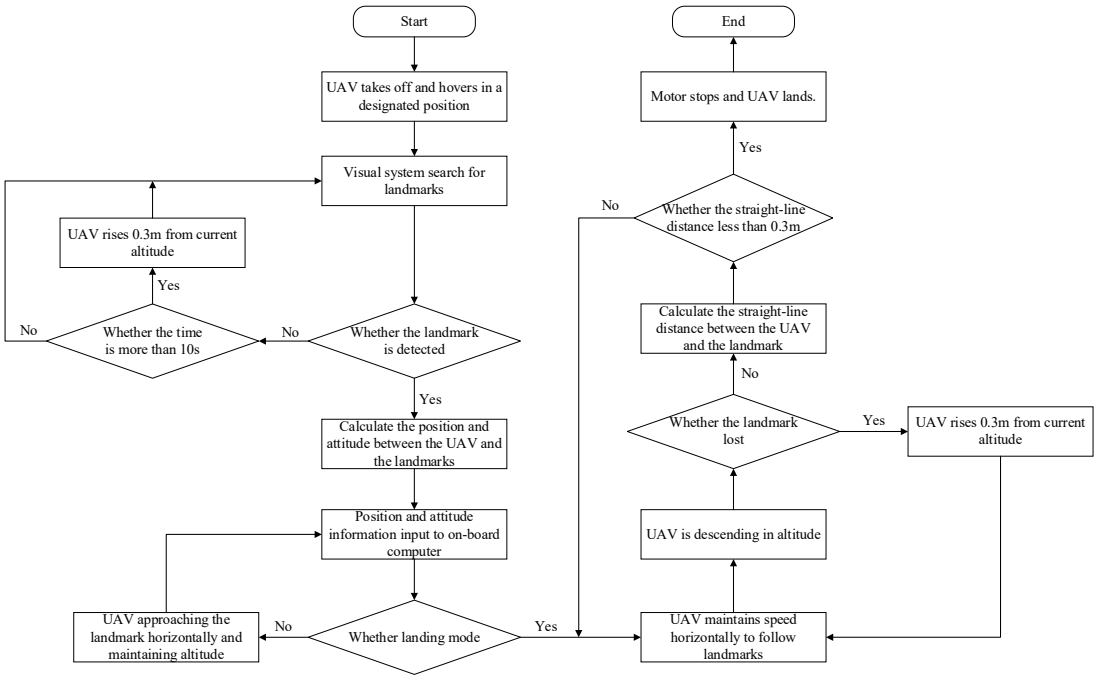

Figure 1. UAV visual tracking landing system control strategy.

Using only visual information for autonomous UAV tracking and landing in GPS-less environments requires both estimating the position and attitude of the UAV itself based on visual navigation techniques, and detecting and tracking landmarks to achieve a landing. Therefore, the UAV has to carry two cameras, the first with a T265 binocular camera from Intel for localization and the second with a monocular camera for target tracking.

In this experimental research, we use the landmark generated by the ArUco library provided by OpenCV to guide the UAV to perform a tracking landing task. The inner and outer nested landmarks were used (shown in Figure 2), the landmarks were parameterized, and landmark parameter optimization experiments were performed to derive the optimal landmark parameters.

(**a**) (**b**)

Figure 2. This is ArUco marker: (**a**) outer marker; (**b**) inner marker.

In the UAV tracking landing missions, landmark failure typically occurs at the time of touchdown. While the relative distance between the UAV and the landmark in the height direction in the landing mode is between 0.3 and 0.6m, the variation of the relative distance between the UAV and the landmark in the landmark parameter optimization experiments is therefore set in the range of 0.3 to 0.6m (shown in Figure 3). The UAV use vision to measure the relative distance between the UAV and inner and outer markers of varying sizes. The position of the UAV does not move, changing

Preprints (www.preprints.org) | NOT PEER-REVIEWED | Posted: 30 October 2023 doi:10.20944/preprints202310.1777.v1

the position of the landmark. The red "x" in the graph indicates each position of the landmark in the experiment, and the results of three experiments were recorded at each position. Table 1 shows the estimated relative distances for inner markers of different sizes. Table 2 shows the estimated relative distances for outer markers of different sizes. Where "-" indicates that the relative distance could not be calculated because the marker was not detected due to camera resolution issues.

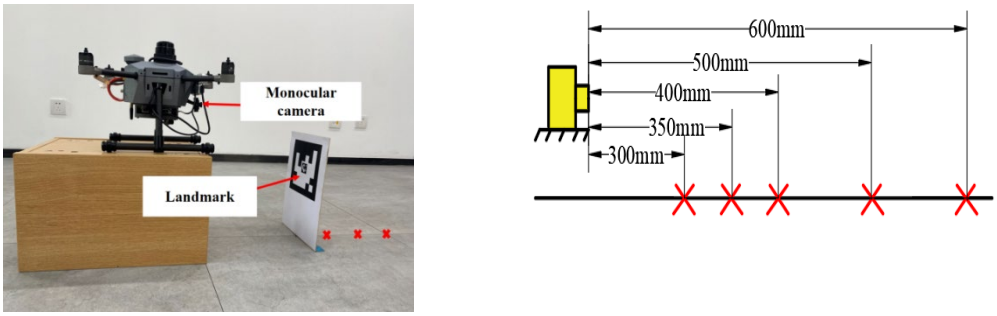

(**a**) (**b**)

Figure 3. Parameter optimization experiment: (**a**) shows the experimental scenario; (**b**) shows the experimental design.

Table 1. Inner ArUco marker different sizes relative distance estimation data.

Size (mm)	Reference Value (mm)	Measured Value1 (mm)	Measured Value2 (mm)	Measured Value3 (mm)	Average Value (mm)	Deviation (mm)
20*20	300	306	310	312	309.3	9.3
	350	-	-	-	-	-
	400	-	-	-	-	-
	500	-	-	-	-	-
	600	-	-	-	-	-
30*30	300	313	312	311	312	12.0
	350	369	366	368	367.7	17.7
	400	426	419	421	422	22.0
	500	-	-	-	-	-
	600	-	-	-	-	-
40*40	300	313	311	313	312.3	12.3
	350	369	366	371	368.7	18.7
	400	426	419	421	423	23.0
	500	524	527	520	523.7	23.7
	600	-	-	-	-	-

Table 2. Outer ArUco marker different sizes relative distance estimation data.

Size (mm)	Reference Value (mm)	Measured Value1 (mm)	Measured Value2 (mm)	Measured Value3 (mm)	Average Value (mm)	Deviation (mm)
100*100	300	305	306	306	306	6
	350	361	360	361	361	11
	400	411	412	413	412	12
	500	517	518	519	518	18
	600	620	623	621	621	21
150*150	300	306	306	306	306	6
	350	359	358	358	358	8
	400	410	411	410	410	10

Preprints (www.preprints.org) | NOT PEER-REVIEWED | Posted: 30 October 2023 doi:10.20944/preprints202310.1777.v1

	500	516	514	515	515	15
	600	621	619	620	620	20
	300	307	307	307	307	7
	350	359	360	358	359	9
200*200	400	410	411	410	410	10
	500	515	514	515	515	15
	600	619	618	618	618	18

To achieve more accurate landings, it is necessary for the relative position estimation data to possess a higher level of accuracy as the distance between the UAV and the landmark decreases. Based on data in the table, the relative distance derived from the inner marker of size 30mm*30mm is closer to the actual value when the relative distance is small. Although the UAV cannot detect the inner marker measuring 30mm*30mm at long distances, it can still obtain relative position information by recognizing the outer marker, which follows the sequence of landmark recognition in real-world scenarios. Choose an outer marker with a size of 150x150mm for more precise relative position estimation at smaller distances. The optimal nested landmark parameters are then determined (shown in Figure 4).

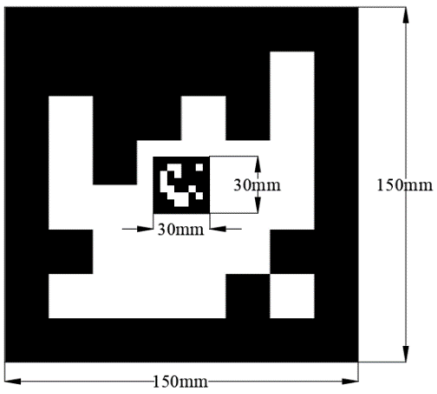

Figure 4. This is a tracking landing landmark.

3. Results

Indoor flight experiments on UAV tracking landings were conducted in this research. The experimental scenario can be seen in Figure 5, which includes a quadcopter UAV with a wheelbase of 450mm, a ground-based UGV, and a landing platform with ArUco marker. The UAV features high-speed monocular and binocular cameras, an on-board processor, the Nvidia-developed Jetson Xavier NX board, and flight controllers utilizing the Pixhawk4 hardware co-created by the PX4 team. A protective net was constructed around the experimental site perimeter, and ArUco markers were affixed to the net to enhance the UAV's positional accuracy. A coordinate system was established at the experimental site, as depicted in Figure 5. Record the offset of the initial UAV and UGV positions from the origin of the defined coordinate system prior to the experiment's commencement. Since the position and attitude transformations of UAV and UGV are based on the body coordinate system, and the position information is recorded with its own starting point as the origin, the position information of the two in the same coordinate system can be obtained by making a difference between the data recorded by the two and the deviation of their respective initial positions.

We conduct experiments to track the flight of ArUco marker that move with the UGV three types of motion: linear reciprocating, circular, and straight-sided elliptical. The UGV was made to move at three speeds, $v1$=0.2m/s, $v2$=0.4m/s, and $v3$=0.6m/s, while performing three different forms of motion in order to test the robustness and accuracy of the UAV's dynamic tracking of landings.

Preprints (www.preprints.org) | NOT PEER-REVIEWED | Posted: 30 October 2023 doi:10.20944/preprints202310.1777.v1

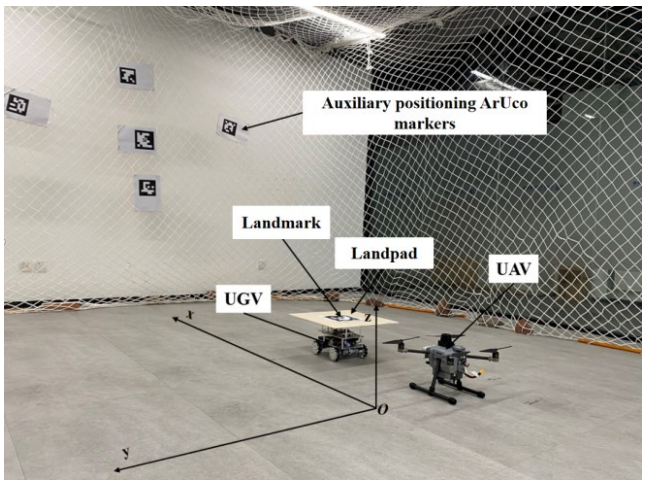

Figure 5. This is the experimental scenario.

3.1. Tracking Experiments

3.1.1. Linear Reciprocating Trajectory

In the experiment, landmarks follow the UGV while it moves in a straight reciprocating motion at three different speeds. This is done to verify the tracking performance of the UAV. Taking into account the influence of the UAV's movement speed and camera field of view on tracking performance, we adjusted the starting point of the UAV's tracking at different heights depending on the speed (shown in Figure 6).

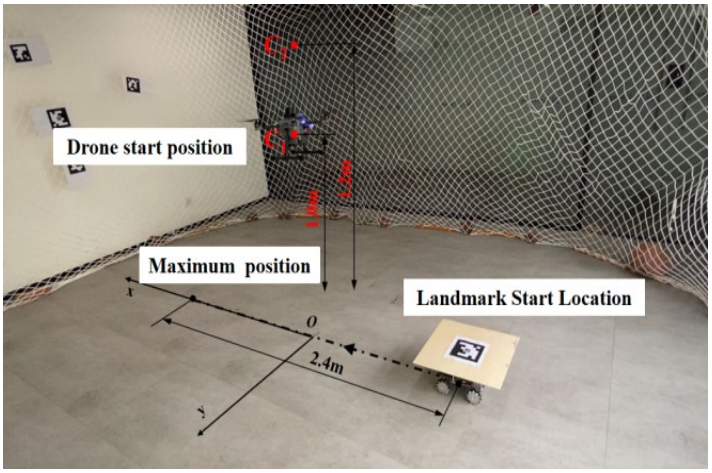

Figure 6. Linear reciprocating tracking experimental environment. C1 represents the initial altitude of the UAV while the UGV is in motion at velocity *v1*. The coordinates of point C1 in space are designated as (0m, 0m,1.0m). C2 is the initial altitude of the UAV while it travels at velocities *v2* and *v3*. The coordinates of C2 are (0m, 0m, 1.2m). In all three velocity changes, the UGV's initial coordinates are consistently (-1.1m, 0m, 0m), while the landmark's initial position is (-1.1m, 0m, 0.3m) due to the landing platform's height being 0.3m from the ground.

When the UGV's is moving at velocity *v1*, the UAV's position relative to the UGV in the x and y axes can be obtained (Figures 7-8). Where x_r and y_r represent the deviations of the UAV and UGV along the x and y axes, respectively. The speeds of the UAV and the UGV on the x and y axes are depicted in Figure 9. There was a momentary increase in the speed of the UAV at 10 seconds, attributed to the landmark entering the UAV's field of view. The UAV's speed overshooting at 18s and 28s recurs as a result of the UGV changing direction. During stable tracking, the UAV's linear

Preprints (www.preprints.org) | NOT PEER-REVIEWED | Posted: 30 October 2023 doi:10.20944/preprints202310.1777.v1

velocities along the x and y axes fluctuate at a rate commensurate with the speed of the UGV motion attachment.

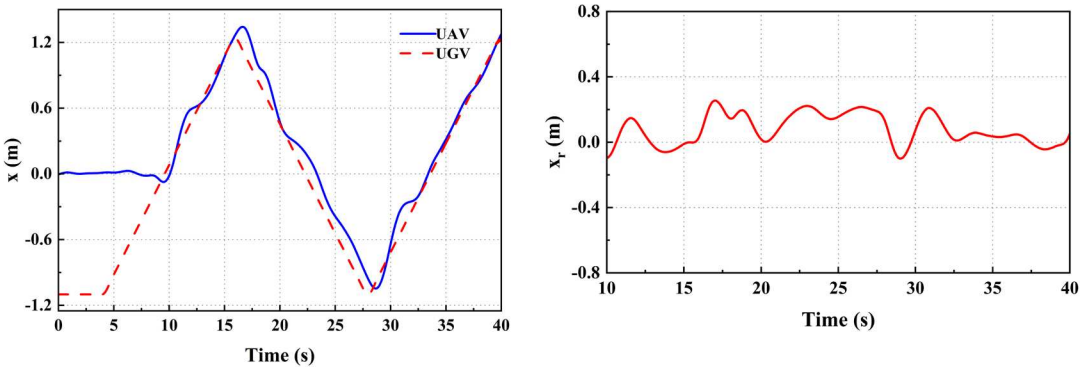

(**a**) (**b**)

Figure 7. UAV x-axis position relationship diagram: (**a**) x-axis absolute position relationship; (**b**) Position deviation in x-axis direction.

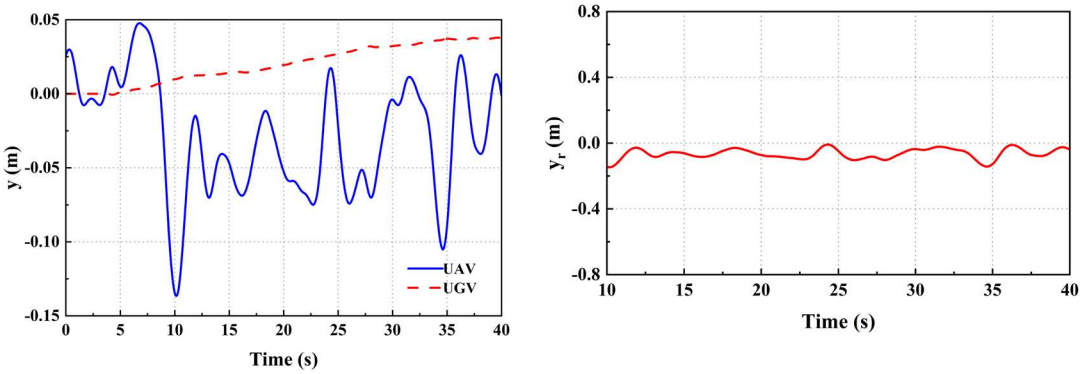

(**a**) (**b**)

Figure 8. UAV y-axis position relationship diagram: (**a**) y-axis absolute position relationship; (**b**) Position deviation in y-axis direction.

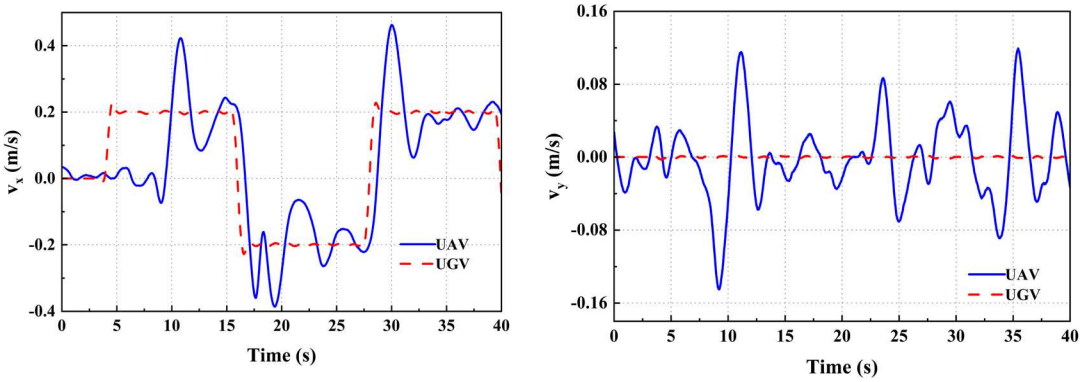

(**a**) (**b**)

Figure 9. UAV and UGV line speed relationship chart: (**a**) x-axis velocity relationship; (**b**) y-axis velocity relationship.

From Figure 10, we are able to obtain the positional deviation of both the UAV and UGV on the x and y axes while the UGV is moving at three distinct speeds, namely x_r and y_r. The UGV's tracking was stable at speed *v1*, but failed to maintain stability for extended durations at speeds *v2* and *v3*. The UAV was more susceptible to losing the target due to the experimental site's limitations. The

Preprints (www.preprints.org) | NOT PEER-REVIEWED | Posted: 30 October 2023 doi:10.20944/preprints202310.1777.v1

UAV flew at a lower altitude, and the camera's field of view was smaller. The mean and the mean square deviation of positional deviations in the x and y axes during constant tracking at speeds *v1* and *v2* were calculated and presented in Table 3. The mean outcomes in the table indicate that there is a slight increase in positional deviation between the UAV and the UGV in both the x and y-axis directions, as the speed of UGV movement increases. However, it still remains at the decimeter level. The table's mean square results indicate a gradual increase in x-axis position deviation fluctuation with the UGV's increasing speed, whereas the UGV's speed does not have a direct relation to y-axis position deviation fluctuation.

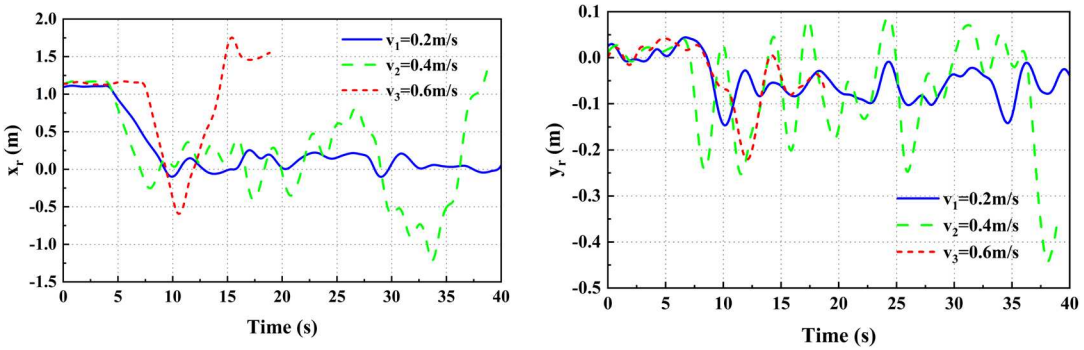

(**a**) (**b**)

Figure 10. Position relationship between UAV and UGV at three speeds: (**a**) x-axis position deviation; (**b**) y-axis position deviation.

Table 3. Mean and mean square deviation of the position deviation of UAV from the UGV.

Velocity	Average Value Error		Mean Square Error	
	x_{AVE}(m/s)	y_{AVE}(m/s)	x_{MSE}(m/s)	y_{MSE}(m/s)
v1	6.73×10^{-2}	2.55×10^{-2}	7.44×10^{-2}	3.08×10^{-2}
v2	4.11×10^{-1}	8.88×10^{-2}	2.75×10^{-1}	6.54×10^{-2}

From Figure 11, one can derive the velocity deviation between the UAV and UGV on the x and y axes, denoted as v_{xr} and v_{yr}, respectively, when the UAV moves at three distinct velocities. The mean squared sum of the difference in velocity between the UAV and the UGV in the x and y axes directions is computed for UGV velocities *v1* and *v2*. The findings are presented in Table 4. When comparing the speed deviation fluctuations near 0m/s at different speeds, it becomes more evident that the fluctuation near 0m/s increases as the mean square sum of the speed deviation increases. As the UGV's speed increases, the mean square sum of the deviation in the x-axis velocity also increases resulting in more noticeable fluctuation. Meanwhile, the y-axis deviation fluctuation remains consistent near the speed of 0 m/s. Throughout the entire tracking process, the speed response of the UAV exhibits no noticeable oscillations and remains consistent with the moving speed of the UGV. This observation suggests that the UAV performs well in tracking. Throughout the entire tracking process, the speed response of the UAV exhibits no noticeable oscillations and remains consistent with the moving speed of the UGV. This observation suggests that the UAV performs well in tracking.

Preprints (www.preprints.org) | NOT PEER-REVIEWED | Posted: 30 October 2023 doi:10.20944/preprints202310.1777.v1

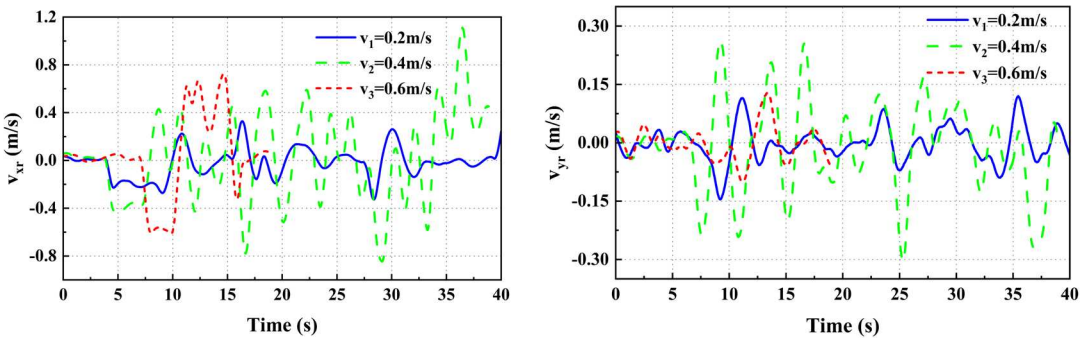

Figure 11. Velocity relationship between UAV and UGV at three speeds: (**a**) x-axis speed deviation; (**b**) y-axis speed deviation.

Table 4. Mean square sum of velocity deviation of UAV and UGV.

Velocity	Mean Square Error	
	$v_{x_{MS}}$(m/s)	$v_{y_{MS}}$(m/s)
v_1	1.30×10^{-2}	1.89×10^{-3}
v_2	1.33×10^{-1}	1.32×10^{-2}

3.1.2. Circular Trajectory

The UAV circular trajectory tracking experiment parallels the linear reciprocating motion tracking experiment. The UGV moves in a circular motion, with a radius of 0.8 meters, at three distinct velocities. Only the starting point coordinates for the UAV and UGV were altered in comparison to the linear reciprocal motion tracking experiment (shown in Figure 12).

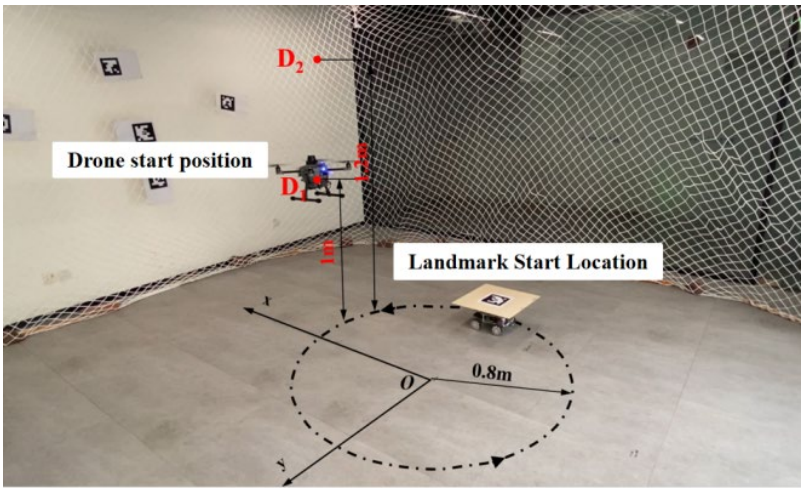

Figure 12. Circular trajectory tracking experimental environment. The starting coordinates of the UGV are consistently (0m, -0.8m, 0m). D1 represents the initial altitude of the UAV when the UGV is in motion at speed *v1*. The coordinates of D1 in space are (0m, 0m, 1.0m). D2 is another initial altitude of the UAV, but this time when the UGV moves at speeds *v2* and *v3*. The coordinates of D2 are (0m, 0m, 1.2m).

We can determine the amount of deviation in position between the UAV and the UGV when the UGV is moving at three distinct speeds (shown in Figure 13). Achieving stable tracking is possible at UGV speeds *v1* and *v2*, however, at speed *v3*, the target is lost around the 15th second, making it impossible to maintain stable tracking for a long time. The probable reason for this is the low flight altitude of the UAV which narrows the field of view of the camera and thereby increases the chances of target loss. The mean and mean square deviation of the position deviation of the UAV and the

Preprints (www.preprints.org) | NOT PEER-REVIEWED | Posted: 30 October 2023 doi:10.20944/preprints202310.1777.v1

UGV are calculated and the results are shown in Table 5. It can be concluded that as the speed of the UGV increases, the mean position error and the mean square error of the x and y axes increase to a certain extent, i.e., the position error and the degree of fluctuation of the position error are positively correlated with the speed of the UGV. Furthermore, when compared with Table 3, the mean value of the x-axis position deviation for the UGV making a circular motion at the same speed is smaller. And since the UGV has a y-axis velocity in the circular motion, the mean and the mean square of the y-axis position deviation are larger in the circular motion.

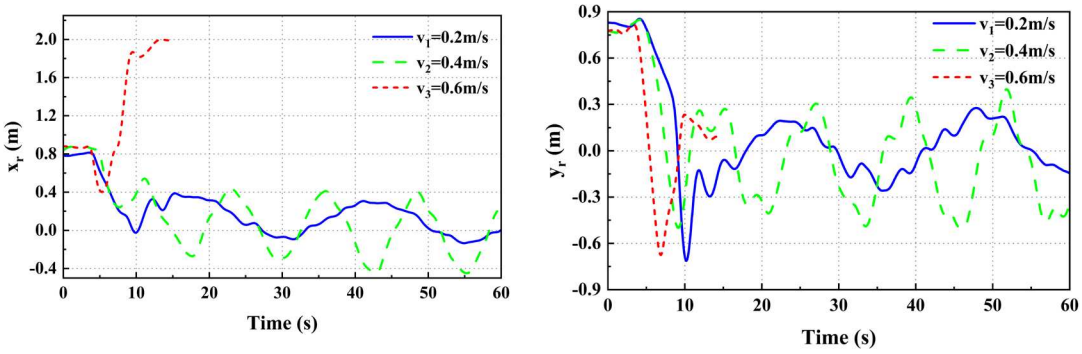

(**a**) (**b**)

Figure 13. Position relationship between UAV and UGV at three speeds: (**a**) x-axis position deviation; (**b**) y-axis position deviation.

Table 5. Mean and mean square deviation of the position deviation of UAV from the UGV.

Velocity	Average Value Error		Mean Square Error	
	x_{AVE}(m/s)	y_{AVE}(m/s)	x_{MSE}(m/s)	y_{MSE}(m/s)
v1	1.65×10^{-1}	1.41×10^{-1}	1.14×10^{-1}	1.02×10^{-1}
v2	2.41×10^{-1}	2.43×10^{-1}	1.35×10^{-1}	1.37×10^{-1}

We can get the velocity deviation between the UAV and the UGV on the x and y axes when the UGV is moving at three different speeds (shown in Figure 14). The mean square sum of the velocity deviations was calculated and the results are shown in Table 6. The fluctuation of UAV and UGV speed deviation becomes more noticeable as the speed of the UGV increases. Compared to Table 4, the fluctuation of the velocity deviation in the x-axis direction is smaller for the same velocity in circular motion. At the same time, since the UGV has a y-axis velocity during its circular motion, the phenomenon of fluctuating velocity deviation in the y-axis direction between the UAV and the UGV is more noticeable.

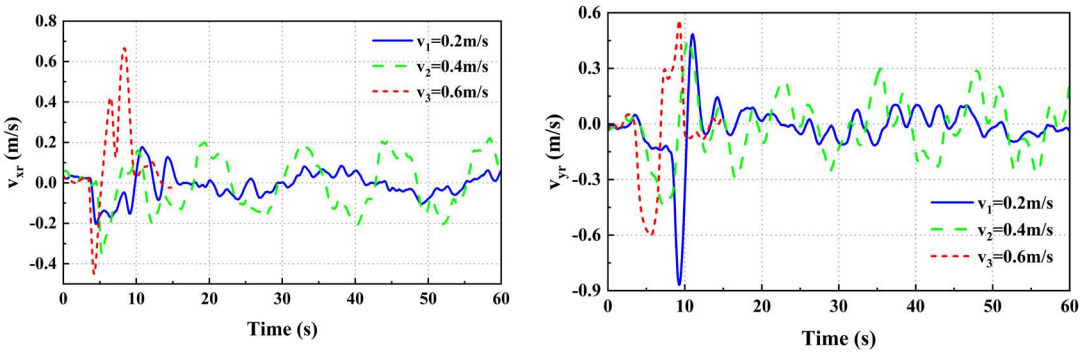

(**a**) (**b**)

Figure 14. Velocity relationship between UAV and UGV at three speeds: (**a**) x-axis speed deviation; (**b**) y-axis speed deviation.

Preprints (www.preprints.org) | NOT PEER-REVIEWED | Posted: 30 October 2023 doi:10.20944/preprints202310.1777.v1

Table 6. Mean square sum of velocity deviation of UAV and UGV.

Velocity	Mean Square Error	
	$v_{x_{MS}}$(m/s)	$v_{y_{MS}}$(m/s)
v_1	2.89×10^{-3}	7.88×10^{-3}
v_2	7.63×10^{-2}	7.55×10^{-2}

As a whole, when the UGV moves at three different speeds, the position deviation of the UAV and the UGV in the x and y axes directions can be kept within the range of ±0.4m under the stable tracking state of the UAV and the velocity deviation of the two in the x and y axes directions basically stays within the ranges of ±0.2m/s, ±0.3m/s, which means that the tracking performance of the UAV is good.

3.1.3. Straight Sided Ellipse Trajectory

Experiments on UAV tracking of UGV moving in a straight elliptical trajectory (shown in Figure 15). Since the results of the previous experiments show that the UAV can realize the tracking of the UGV when it is moving at three speeds, the experiments are conducted only for the UGV moving at speed *v1* when the UGV is moving in a straight-sided elliptical trajectory.

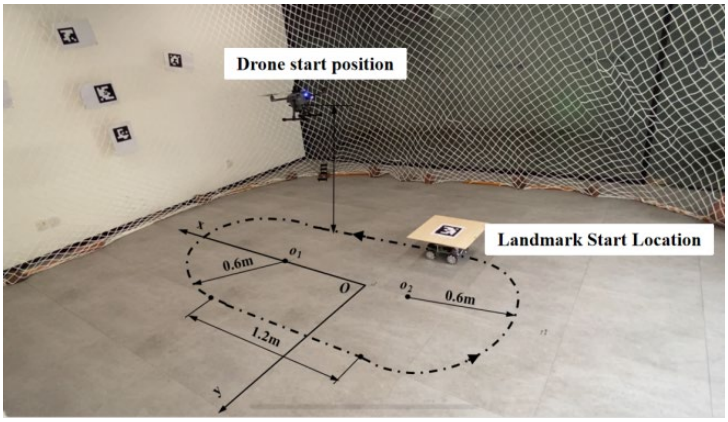

Figure 15. Straight sided ellipse trajectory tracking experimental environment. The coordinates of the UAV tracking start point are (0.9m, -0.6m, 1.0m) and the coordinates of the UGV start point are (-0.3m, -0.6m, 0m).

We can obtain the position and velocity deviation of the UAV and the UGV when the UGV moves in a straight-sided ellipse with velocity *v1* (Figures 16 and 17). The position deviation between the UAV and the UGV in the x and y axes directions is always within the range of ±0.4m, and the speed deviation in the x and y axes directions is always within the range of ±0.15m/s, which indicates that the tracking performance of the UAV for the complex trajectory is still good.

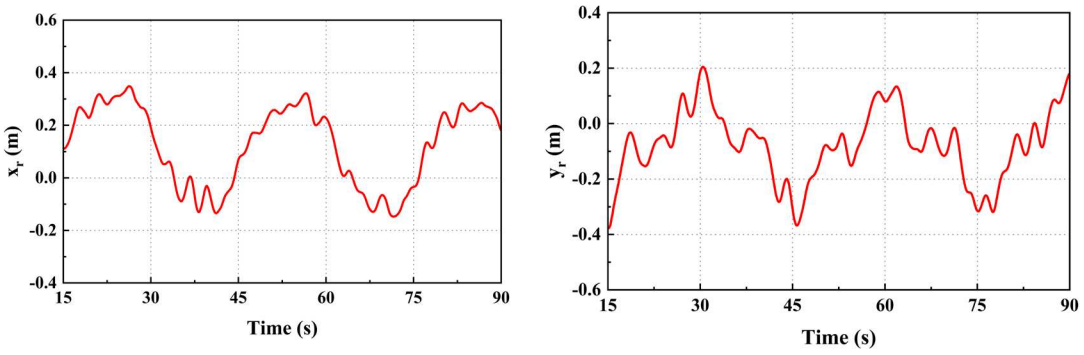

(**a**) (**b**)

Preprints (www.preprints.org) | NOT PEER-REVIEWED | Posted: 30 October 2023 doi:10.20944/preprints202310.1777.v1

Figure 16. Position deviation of UAV from UGV: (**a**) x-axis position deviation; (**b**) y-axis position deviation.

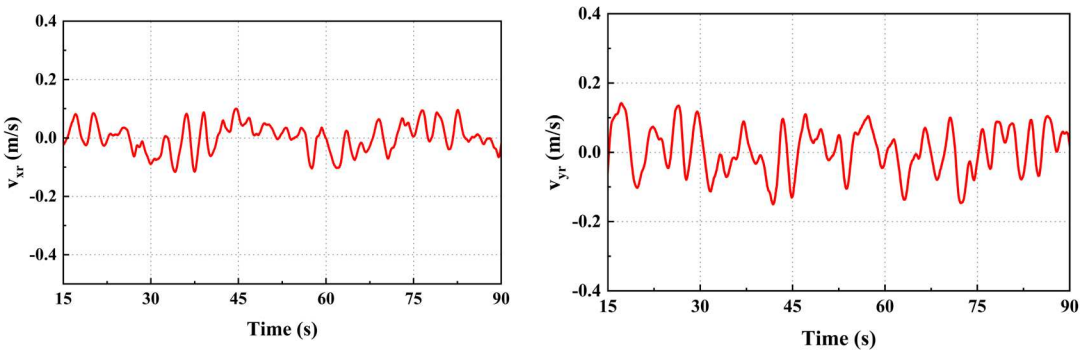

(**a**) (**b**)

Figure 17. Speed deviation of UAV from UGV: (**a**) x-axis velocity deviation; (**b**) y-axis velocity deviation.

3.2. Landing Experiments

To further verify the landing performance of the UAV, we conducted landing experiments in static and dynamic scenarios (shown in Figure 18). We expect the horizontal landing accuracy to be no more than 0.5m. In the stationary landmark landing experiment, the UAV ascends to a specific altitude and initiates a tracking landing mission once the landmark enters the field of view of the UGV. To minimize the possibility of error, we replicated three experiments and tabulated the x and y axes position coordinates and averaged values from each experiment in Table 7. In the dynamic landing experiment, the UGV moves linearly along the x-axis at three different speeds, while the UAV performs dynamic tracking and landing experiments on the UGV. When the landmark enters the monocular camera's field of view, the UAV initiates the tracking landing mission. The UAV horizontally approaches the landmark while computing its relative position and attitude. Additionally, it adjusts its speed to match that of the UGV. As the UAV reduces its flight altitude, it measures its distance from the center of landmark d. When the relative position of the two meets the landing conditions, the UAV enters the landing mode. When the distance, d, is less than or equal to 0.3 meters, the on-board processor will send a command to the UAV flight controller to land. The motor will stop and the UAV will land on the UGV. Table 8 displays the dynamic landing accuracy of the UAV at three separate vehicle speeds. The results of the experiment indicate that the UAV's static landing accuracy can achieve a range between 0.03 and 0.04 meters. During dynamic landing scenarios, the UAV demonstrated an x-axis landing accuracy of 0.23 meters and a y-axis landing accuracy of 0.2 meters, which is consistent with the predetermined expectations and satisfies the landing accuracy requirements.

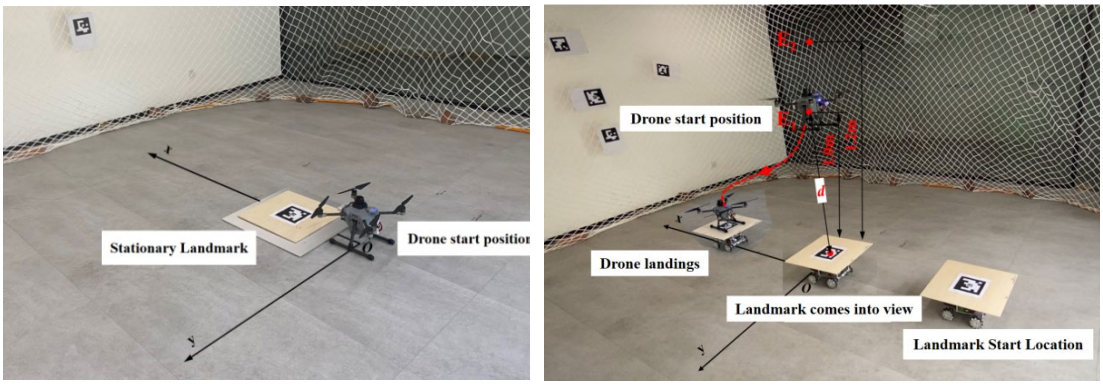

(**a**) (**b**)

 doi:10.20944/preprints202310.1777.v1

Figure 18. UAV landing experiment environment: (**a**) Static experimental environment, the landmark coordinate point is (0.48m, 0m, 0m) and the UAV start point is (0m, 0m, 0m); (**b**) Dynamic experimental environment, E1 serves as the initial altitude for the UAV when the UGV is traveling at speed *v1*. The coordinates of E1 in space are (0.0m, 0.0m, 1.0m). On the other hand, when the UGV is moving at speeds *v2* and *v3*, E2 serves as the starting altitude point of the UAV, and its coordinates are (0.0m, 0.0m, 1.2m). It is worth noting that the UGV starting coordinates remain constant at (-1.1m, 0m, 0m) regardless of the speed.

Table 7. Static landing experiment accuracy and its mean value.

Experimental Sequence	x-Axis Landing Accuracy (m)	y-Axis Landing Accuracy (m)
Test 1	0.05	0.04
Test 2	0.01	0.04
Test 3	0.04	0.05
Average value	0.03	0.04

Table 8. Dynamic landing experiment accuracy and its mean value.

Velocity	x-Axis Landing Accuracy (m)	y-Axis Landing Accuracy (m)
v1	0.14	0.04
v2	0.23	0.01
v3	0.32	0.01
Average value	0.23	0.20

4. Discussion

During the experiment, the UAV was unable to track for an extended period when the UGV was moving at velocity *v3*. This limitation can be attributed to the low flight altitude of the UAV and site constraints causing the camera to capture an insufficient image, hence increasing the likelihood of loss of the target. In this research, the structural design of the ArUco marker and dimension parameter optimization improved the system's robustness to recognize landmarks to some extent. However, it fails to consider the UAV control strategy in situations when the target becomes occluded or is lost for an extended period during the tracking process. Subsequent research can utilize this as a starting point to enhance the system's ability to identify and track targets with greater accuracy and efficacy.

5. Conclusions

In this paper, we propose a method for tracking and landing UAVs in dynamic environments using nested ArUco marker. Firstly, this study examines tracking and landing as a unified process and proposes a switching strategy for transitioning between tracking and landing modes. Our proposed inner and outer loop controllers, which combine serial PID and fuzzy algorithms, effectively control a quadrotor UAV. Relative position and attitude estimation and landmark recognition detection relying only on vision. Mode conversion of the UAV for dynamic tracking and landing tasks is achieved by calculating the relative positional information between the UAV and the UGV using landmarks. Second, two landmarks with varying sizes were created as nested landmark codes to aid the UAV in tracking and positioning the UGV, taking into account the correlation between ArUco marker size and positioning accuracy. The experiments yielded the optimal landmark size parameters for enhancing the robustness of landmark classification to meet the task requirements. Finally, tracking and landing experiments were conducted at three different speeds. Overall, our adopted method improves the accuracy and robustness of tracking and landing during the dynamic tracking and landing process of UAV on UGV with varying motion trajectories.

Furthermore, our method demonstrates higher landing accuracy against the dynamic landing platform, providing evidence for its feasibility in dynamic tracking and landing of UAV.

Author Contributions: Conceptualization, H.Z.; Methodology, B.W.; Validation, B.W. and R.M.; Data curation, B.W.; Writing—original draft preparation, B.W. and R.M.; Writing—review and editing, H.Z., T.Y. and Y.S.; Supervision, H.Z.; Project administration, H.Z.; Funding acquisition, H.Z. All authors have read and agreed to the published version of the manuscript.

Funding: This research was funded by Jilin Provincial Development and Reform Commission Industrial Technology Research and Development Program in 2020, grant number 2020C018-2.

Data Availability Statement: The data used to support the findings of this research are available from the corresponding author upon request.

Conflicts of Interest: The authors declare no conflict of interest.

References

1. Al-Ghussain, L.; Bailey, S.C.C. Uncrewed Aircraft System Measurements of Atmospheric Surface-Layer Structure During Morning Transition. *Bound.-Layer Meteor.* **2022**, *185*, 229-258, doi:10.1007/s10546-022-00729-2.
2. Greco, R.; Barca, E.; Raumonen, P.; Persia, M.; Tartarino, P. Methodology for measuring dendrometric parameters in a mediterranean forest with UAVs flying inside forest. *Int. J. Appl. Earth Obs. Geoinf.* **2023**, *122*, 13, doi:10.1016/j.jag.2023.103426.
3. Abrahams, M.; Sibanda, M.; Dube, T.; Chimonyo, V.G.P.; Mabhaudhi, T. A Systematic Review of UAV Applications for Mapping Neglected and Underutilised Crop Species’ Spatial Distribution and Health. *Remote Sensing* **2023**, *15*, 4672.
4. Sanchez-Lopez, J.L.; Pestana, J.; Saripalli, S.; Campoy, P. An Approach Toward Visual Autonomous Ship Board Landing of a VTOL UAV. *J. Intell. Robot. Syst.* **2014**, *74*, 113-127, doi:10.1007/s10846-013-9926-3.
5. Michael, N.; Shen, S.J.; Mohta, K.; Mulgaonkar, Y.; Kumar, V.; Nagatani, K.; Okada, Y.; Kiribayashi, S.; Otake, K.; Yoshida, K.; et al. Collaborative mapping of an earthquake-damaged building via ground and aerial robots. *J. Field Robot.* **2012**, *29*, 832-841, doi:10.1002/rob.21436.
6. Miki, T.; Khrapchenkov, P.; Hori, K.; Ieee. UAV/UGV Autonomous Cooperation: UAV assists UGV to climb a cliff by attaching a tether. In Proceedings of the IEEE International Conference on Robotics and Automation (ICRA), Montreal, CANADA, May 20-24, 2019; pp. 8041-8047.
7. Sanchez-Lopez, J.L.; Castillo-Lopez, M.; Olivares-Mendez, M.A.; Voos, H. Trajectory Tracking for Aerial Robots: an Optimization-Based Planning and Control Approach. *J. Intell. Robot. Syst.* **2020**, *100*, 531-574, doi:10.1007/s10846-020-01203-2.
8. Kassab, M.A.; Maher, A.; Elkazzaz, F.; Zhang, B.C.; Ieee. UAV TARGET TRACKING BY DETECTION VIA DEEP NEURAL NETWORKS. In Proceedings of the IEEE International Conference on Multimedia and Expo (ICME), Shanghai, PEOPLES R CHINA, Jul 08-12, 2019; pp. 139-144.
9. Elloumi, M.; Escrig, B.; Dhaou, R.; Idoudi, H.; Saidane, L.A.; Ieee. Designing an energy efficient UAV tracking algorithm. In Proceedings of the 13th International Wireless Communications and Mobile Computing Conference (IWCMC), Valencia, SPAIN, Jun 26-30, 2017; pp. 127-132.
10. Altan, A.; Hacioglu, R. Model predictive control of three-axis gimbal system mounted on UAV for real-time target tracking under external disturbances. *Mech. Syst. Signal Proc.* **2020**, *138*, 23, doi:10.1016/j.ymssp.2019.106548.
11. Jin, S.G.; Zhang, J.Y.; Shen, L.C.; Li, T.X. On-board Vision Autonomous Landing Techniques for Quadrotor: A Survey. In Proceedings of the 35th Chinese Control Conference (CCC), Chengdu, PEOPLES R CHINA, Jul 27-29, 2016; pp. 10284-10289.
12. Nepal, U.; Eslamiat, H. Comparing YOLOv3, YOLOv4 and YOLOv5 for Autonomous Landing Spot Detection in Faulty UAVs. *Sensors* **2022**, *22*, 15, doi:10.3390/s22020464.
13. Zhang, H.T.; Hu, B.B.; Xu, Z.C.; Cai, Z.; Liu, B.; Wang, X.D.; Geng, T.; Zhong, S.; Zhao, J. Visual Navigation and Landing Control of an Unmanned Aerial Vehicle on a Moving Autonomous Surface Vehicle via Adaptive Learning. *IEEE Trans. Neural Netw. Learn. Syst.* **2021**, *32*, 5345-5355, doi:10.1109/tnnls.2021.3080980.
14. Abujoub, S.; McPhee, J.; Westin, C.; Irani, R.A.; Ieee. Unmanned Aerial Vehicle Landing on Maritime Vessels using Signal Prediction of the Ship Motion. In Proceedings of the Conference on OCEANS MTS/IEEE Charleston, Charleston, SC, Oct 22-25, 2018.
15. Li, W.Z.; Ge, Y.; Guan, Z.H.; Ye, G. Synchronized Motion-Based UAV-USV Cooperative Autonomous Landing. *J. Mar. Sci. Eng.* **2022**, *10*, 19, doi:10.3390/jmse10091214.

16. Persson, L.; Muskardin, T.; Wahlberg, B.; Ieee. Cooperative Rendezvous of Ground Vehicle and Aerial Vehicle using Model Predictive Control. In Proceedings of the 56th Annual IEEE Conference on Decision and Control (CDC), Melbourne, AUSTRALIA, Dec 12-15, 2017.
17. Araar, O.; Aouf, N.; Vitanov, I. Vision Based Autonomous Landing of Multirotor UAV on Moving Platform. *J. Intell. Robot. Syst.* **2017**, *85*, 369-384, doi:10.1007/s10846-016-0399-z.
18. Borowczyk, A.; Nguyen, D.T.; Nguyen, A.P.V.; Nguyen, D.Q.; Saussié, D.; Le Ny, J. Autonomous Landing of a Multirotor Micro Air Vehicle on a High Velocity Ground Vehicle. In Proceedings of the 20th World Congress of the International-Federation-of-Automatic-Control (IFAC), Toulouse, FRANCE, Jul 09-14, 2017; pp. 10488-10494.
19. Xu, Y.B.; Liu, Z.H.; Wang, X.K. Monocular Vision based Autonomous Landing of Quadrotor through Deep Reinforcement Learning. In Proceedings of the 37th Chinese Control Conference (CCC), Wuhan, PEOPLES R CHINA, Jul 25-27, 2018; pp. 10014-10019.
20. Li, W.J.; Fu, Z.Y. Unmanned aerial vehicle positioning based on multi-sensor information fusion. *Geo-Spat. Inf. Sci.* **2018**, *21*, 302-310, doi:10.1080/10095020.2018.1465209.
21. Lim, J.; Lee, T.; Pyo, S.; Lee, J.; Kim, J.; Lee, J. Hemispherical InfraRed (IR) Marker for Reliable Detection for Autonomous Landing on a Moving Ground Vehicle From Various Altitude Angles. *IEEE-ASME Trans. Mechatron.* **2022**, *27*, 485-492, doi:10.1109/tmech.2021.3066643.
22. Yuan, B.X.; Ma, W.Y.; Wang, F. High Speed Safe Autonomous Landing Marker Tracking of Fixed Wing Drone Based on Deep Learning. *IEEE Access* **2022**, *10*, 80415-80436, doi:10.1109/access.2022.3195286.
23. de Croon, G.; Ho, H.W.; De Wagter, C.; van Kampen, E.; Remes, B.; Chu, Q.P. Optic-flow based slope estimation for autonomous landing. *Int. J. Micro Air Veh.* **2013**, *5*, 287-297, doi:10.1260/1756-8293.5.4.287.